Simulations of heating and electron energy distributions in optical field ionized plasmas

T. Ditmire
Imperial College of Science, Technology and Medicine, Prince Consort Road, London SW7 2BZ, United Kingdom
(Received 22 April 1996)

The heating in underdense plasmas produced by optical field ionization and the resulting electron energy distributions have been calculated using Monte Carlo simulations. Though the magnitude of collisional heating is found to be low in plasmas with densities of interest for recombination x-ray lasers, the effect of electron-ion collisions on the shape of the electron energy distribution is important. The consequences that the calculated energy distributions have on three-body recombination rates are found to be dramatic. [S1063-651X(96)07911-1]

PACS number(s): 52.25.Jm, 32.80.Rm, 52.40.Nk, 52.50.Jm

With the current interest and research activity directed toward producing a recombination x-ray laser from an optically ionized plasma, understanding of heating mechanisms in an underdense plasma produced by a short, ionizing laser pulse has become important. The recent success at demonstrating gain in such a recombination system has added greater impetus to studies of heating mechanisms [1,2]. A number of previous theoretical works have addressed the problem of heating in an underdense plasma by a short pulse [3–6]. These works have indicated that the most important heating mechanisms in most cases in these plasmas is above threshold ionization (ATI) and, to a lesser extent, collisional inverse bremsstrahlung when the plasma ion density is above about 10^{19} cm^{-3} [5,6]. Recent experimental work has confirmed these predictions to some extent [7–9]. In calculating the magnitude of the collisional heating the electron energy distribution is often assumed to be Maxwellian [5,10]. Some recent experimental reports, however, indicate that the assumption of a Maxwellian distribution is not justified. Glover *et al.* recently measured the electron energy distributions produced by the field ionization of helium at a density of 10^{18} cm^{-3} with a 616 nm 100 fs pulse [9]. Though the temperature measured in this work matched calculation, the resulting energy distribution within the first 50 ps after the laser ionization was found to be non-Maxwellian.

Experimental results on the recombination time and observed Lyman α gain in lithium have also been inconsistent with most calculations of the plasma heating. Fast recombination ($<$25 ps) of Li ionized by a 400 nm, 100 fs pulse has been observed by Donnelly *et al.* [2] and gain reported on the $n=2\rightarrow1$ transition is unusually high [1,11,12]. It has been suggested in Ref. [11] that this behavior may be due to the non-Maxwellian character of the electron energy distribution immediately after ionization. In that work it was surmised that some of the electrons produced during optical ionization were quite cold ($<$10 eV) and that the rapid recombination and high observed gain were due to the enhanced recombination rate of this cold component in the electron energy distribution. In this paper calculations of electron heating in low density ($<10^{20}$ cm^{-3}) plasmas produced by the tunnel ionization of an intense, femtosecond laser pulse are presented in an attempt to illuminate some of these recently reported results.

The model presented here was developed to examine the effects of ATI and inverse bremsstrahlung on the residual temperatures and the electron energy distributions of short pulse produced plasmas. In this model the plasma is considered to be uniform. Consequently, no space-charge or collective plasma effects are considered. Penetrante and Bardsley recently suggested that space-charge effects can be an important mechanism in short pulse ionized plasmas [4]. However, Pulsifer *et al.* showed that these effects are only important for an electron density $n_e > 0.1 n_{\rm crit}$ (i.e., greater than about 10^{20} cm^{-3}) [10], a density greater than that encountered in most experiments and higher than the densities considered here. The effects of stimulated Raman scattering (SRS) on the plasma heating are also ignored in the model. It has been shown both theoretically as well as experimentally that SRS heating is not important for subpicosecond pulses with intensity below 10^{17} W/cm^2 [13,8,14].

ATI heating is included in the calculation by using the quasistatic model [3]. The ionization is taken to be by pure tunnel ionization in a linearly polarized laser field. The ionization rate equations are solved for an oscillating field with a Gaussian pulse envelope. It is assumed that the ionization rate is given by the static field tunnel ionization formula of Ammosov, Delone, and Krainov [15]:

$$W_{\rm tun} = \frac{\omega_a}{2} \frac{(2l+1)(l+|m|)!}{2^{|m|}|m|!(l+|m|)!} \left(\frac{2e}{n^*}\right)^{2n^*} \frac{1}{2\pi n^*} \frac{I_p}{I_{\rm H}} \times \left[2\left(\frac{I_p}{I_{\rm H}}\right)^{3/2} \frac{\varepsilon_a}{\varepsilon_0}\right]^{2n^*-|m|-1} \exp\left[-\frac{2}{3}\left(\frac{I_p}{I_{\rm H}}\right)^{3/2} \frac{\varepsilon_a}{\varepsilon_0}\right], \quad (1)$$

where I_p is the atom ionization potential, $I_{\rm H}$ is hydrogen's ionization potential ($=13.6$ eV), ω_a is the atomic unit of frequency ($=4.1\times10^{16}$ s^{-1}), ε_0 is the laser field strength, ε_a is the atomic field strength ($=5.1\times10^9$ V/cm), l and m are the angular momentum quantum numbers (the rate is averaged over m for a shell), and n^* is the effective principal quantum number, $n^* = Z(I_p/I_{\rm H})^{-1/2}$. When the ionization rate becomes significant for a certain charge state, a number of test particles are generated at the time step of ionization with each test electron weighted according to the ionization probability at the time in which it is born. The velocities of

these test electrons are then calculated in the oscillating laser field. The residual drift energy of the tunnel ionized electrons after the laser pulse has passed is the ATI energy. The kinetic energy gained in this quasistatic model is [3]

$$E_{\mathrm{ATI}}=2U_p\sin\Delta\phi, \tag{2}$$

where U_p is the electron ponderomotive quiver energy at the time of ionization: $U_p\approx 9.3\times 10^{-14} I(\mathrm{W/cm^2})[\lambda(\mu\mathrm{m})]^2$, and $\Delta\phi$ is the phase off of the peak of the oscillation at which the electron is born. Because the tunnel ionization rate is very nonlinear with the field magnitude, the ionization rate is strongly peaked at a value of $\Delta\phi=0$ and the electron energy distribution in the absence of any collisions is peaked at a kinetic energy of zero [3].

The calculations described in this paper were conducted assuming that the laser pulse is Gaussian in time. It has been previously shown that the pulse shape can have an important effect on the value of the residual ATI energy of the electrons [6]. In particular, it was found that the rise time of the pulse can affect the final residual drift energy of the electrons by a significant amount, with a faster pulse rise time resulting in higher plasma temperatures [6]. For simplicity, however, only symmetric, Gaussian pulses are considered here since such pulse shapes most closely approximate the actual pulses used in most experiments involving femtosecond lasers [1,2,7–9].

The effects of inverse bremsstrahlung on the test particles oscillating during the pulse in the model are included using Monte Carlo methods. The impact approximation for the classical electron-ion collisions is utilized [16]. A maximum impact parameter $b_{\max}$ for calculating the probability for collisions is set by the requirement that a collision occur on a time short compared with a laser oscillation, $b_{\max}=v/\omega$. The results were found to be quite insensitive to the actual value of $b_{\max}$ chosen. As the tunnel ionization proceeds during the laser pulse, the model generates 10 000–20 000 test particles, depending upon the atomic species and pulse peak intensity. This number is large enough to provide good statistics for the heating collisions. The probability of an electron-ion collision is calculated for each test particle at each point in time during the laser pulse and a series of random numbers determines whether a collision occurs and the angle through which the electron is deflected if one does occur.

In this model electron-electron collisions are ignored. In general, this is not necessarily a good approximation in the cold plasmas produced by optical field ionization. However, during the laser pulse, the electrons have kinetic energy of the order of the ponderomotive potential U_p. Therefore even the ''cold'' electrons, those with very little random kinetic energy, have a sizable kinetic energy (>100 eV for intensity of above 10^{15} W/cm^2 in a pulse with a wavelength of 800 nm). Consequently, in the laser field the electron-electron collision rate is lowered. We can ascertain the validity of ignoring electron-electron collisions during the laser pulse by considering the electron-electron collisional relaxation time. This relaxation time is given roughly as [17]

$$t_{ee}=\frac{3\sqrt{6}m_e^{1/2}(kT_e)^{3/2}}{8\pi n_e e^4\ln\Lambda}, \tag{3}$$

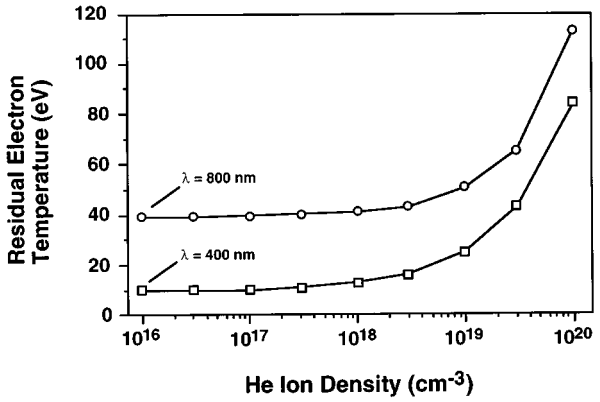

FIG. 1. Calculated temperature of a helium plasma as a function of initial He density ionized by a 100 fs pulse focused to 2×10^{16} W/cm^2, with wavelength of 400 and 800 nm.

where n_e is the electron density and kT_e is the characteristic temperature of the electrons. ln Λ is the Coulomb logarithm ($\approx$4–8 for the low density plasmas considered here [17]). For cold electrons, in the absence of the laser field, this relaxation time is fast. It is approximately 200 fs for electrons with $kT_e=10$ eV and an electron density of 10^{19} cm^{-3}. During the laser pulse, however, it is necessary to account for the oscillatory energy of the electrons. When the intensity is high, the electron kinetic energy is high and this relaxation time is substantially longer. To roughly estimate the relaxation time we can replace kT_e with the ponderomotive energy U_p in Eq. (3). Thus in an 800 nm pulse with an intensity of 10^{16} W/cm^2 the relaxation time is closer to ~100 ps, much longer than the pulses considered in this work. For this reason, the electron-electron relaxation can be ignored in calculating the electron energy distributions that result immediately at the end of the laser pulse.

For the sake of illustration, the predicted electron temperatures and energy distributions for 100 fs pulses (full width at half maximum) will be considered. This closely approximates the conditions of a number of recent experiments in helium and lithium [2,7,9]. Throughout this paper the plasma temperature is defined as $kT_e=2/3\langle E\rangle_{\mathrm{avg}}$ where $\langle E\rangle_{\mathrm{avg}}=\int Ef(E)dE/\int f(E)dE$. First the calculated temperature of a helium plasma produced by a 100 fs pulse focused to 2×10^{16} W/cm^2, an intensity sufficient to completely ionize helium on the rising part of the pulse, is considered. The predicted temperature of 400 and 800 nm wavelength pulses (the fundamental and second harmonic of a Ti:sapphire laser) as a function of ion density is shown in Fig. 1. At an atom density below about 10^{19} cm^3 the temperature is largely determined by the single atom ATI temperature, which in this case is about 10 eV for 400 nm light and 40 eV for 800 nm light. Hence the temperature is largely independent of density. The predicted temperature in He at a density of 10^{18} cm^{-3} (41 eV) is in good agreement with experimentally determined average temperature measured by Glover *et al.* in a He plasma produced with a 120 fs, 800 nm laser [7]. Only when the atom density is above 10^{19} cm^{-3} does the heating from collisions play an important role. Above this density the temperature rises rapidly due to the collisional heating. This rise in temperature is also in qualitative agreement with the measurements of Ref. [8].

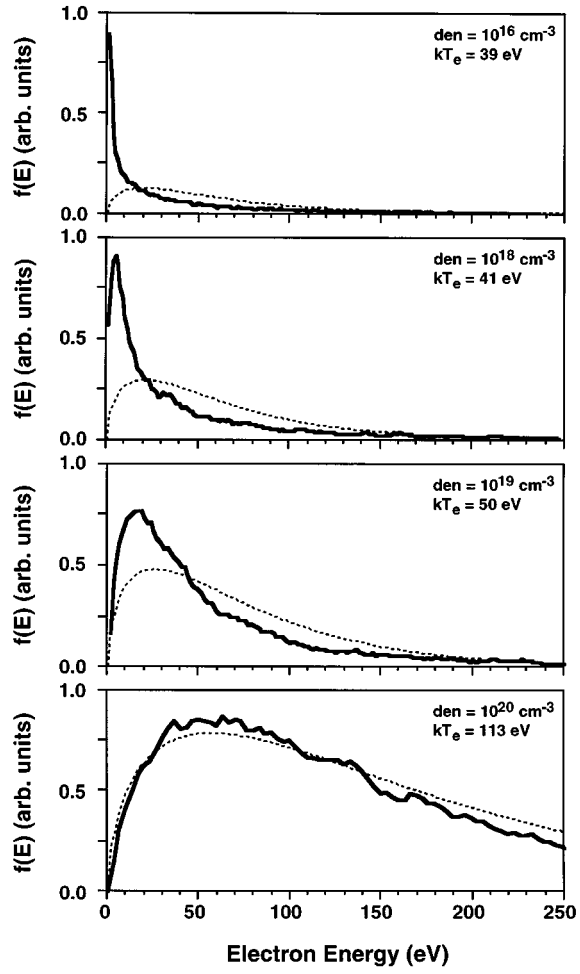

FIG. 2. Calculated electron energy distributions for densities of 10^{17}, 10^{18}, 10^{19}, and 10^{20} cm^{-3} for a helium plasma produced by an 800 nm, 100 fs pulse focused to 2×10^{16} W/cm^2. The solid lines are the Monte Carlo calculations and the dashed lines are Maxwellian distributions with the same average energy as the calculated distribution. All distributions have been normalized such that $\int f(E)dE=1$.

The role of the collisional heating at lower density, however, becomes manifest when the electron energy distribution function for various initial atom densities is considered. Figure 2 illustrates the calculated electron energy distributions produced in a He plasma by an 800 nm, 100 fs pulse focused to 2×10^{16} W/cm^2 with ion densities of 10^{16}, 10^{18}, 10^{19}, and 10^{20} cm^{-3}. At the lowest density, the temperature and the distribution function are characteristic of the single atom ATI distribution. Here, the distribution function is strongly peaked near $E=0$. However, as the atom density is increased, collisions become more important. The non-Maxwellian character of the electron distribution evolves into a Maxwellian distribution at the highest density of 10^{20} cm^{-3} due to the increasing importance of collisional heating of the coldest ATI electrons. The evolution toward a Maxwellian at the highest density is also consistent with the predictions of Jones and Lee which indicated that the solution of the electron distribution function heated by inverse bremsstrahlung in the high field limit is that of a Maxwellian [18]. However, even at lower density, the cold electrons at $E=0$ shift to higher energy, resulting in the intermediate distributions found at density of 10^{18} and 10^{19} cm^{-3}.

This change in the shape of the distribution is a consequence of the electron-ion collisions in the laser field. In the absence of a laser field, the electron-ion collisions are nearly elastic and they are inefficient in altering the shape of the electron energy distribution. However, when the laser field is present, the electron-ion collisions couple energy from the laser into electron thermal energy. The shift in the energy distributions seen in Fig. 2 results from the fact that the laser deposits energy into the colder electrons slightly faster than it heats the hot (>100 eV) electrons. The origin of this energy shift can be seen by considering the collision frequency [19]

$$\nu_{ei}=\frac{4\sqrt{2\pi}Z^2e^4n_e\ln\Lambda}{3m_e^{1/2}}\left(\frac{1}{kT_e+2U_p/3}\right)^{3/2}. \tag{4}$$

(Here the correction factor for the collision frequency in high laser fields of Schlessinger and Wright has been used [19].) From this expression it can be seen that the collision frequency drops as the thermal energy of the electrons rises. For example, in a laser intensity of 10^{16} W/cm^2 and a laser wavelength of 800 nm, the collision frequency of 10 eV electrons is 35% higher than that of 100 eV electrons. Consequently, at the higher density, the strong peak with $E<10$ eV seen in Fig. 2 at the lowest densities moves to higher energy faster than the hot tail.

From Fig. 2 it is clear that even when the total temperature of the plasma is not affected by collisional heating, the shape of the distribution can be strongly affected. The results presented in Fig. 2 for a density of 10^{18} cm^{-3} appear to be in qualitative agreement with the experimental result of Glover *et al.* [9]. In their experiment they found that the heating in a helium plasma by a 100 fs, 616 nm pulse was consistent with ATI heating alone, in keeping with the calculations presented in Fig. 1. The observed energy distribution, however, was not characteristic of either a typical ATI distribution or a Maxwellian. The calculated distribution in Fig. 2 at a density of 10^{18} cm^{-3}, in fact, bears many similarities to the distribution presented in Ref. [9], such as a more strongly peaked shape than a Maxwellian with the peak centered around 10 eV.

The non-Maxwellian character of the calculated distributions at lower density seen in Fig. 2 can have an important effect on the recombination rate of the plasma immediately after creation by the laser pulse. The three-body recombination rate scales quite strongly with electron kinetic energy. Thus the shift of the cold electrons away from the ATI peak at $E=0$ toward a Maxwellian distribution at a density between 10^{17} and 10^{19} cm^{-3} will have a dramatic effect on the recombination rate, despite the fact that the temperature of the plasma does not change significantly. This effect will be particularly important in the context of recombination x-ray laser experiments recently carried out in Li [1,2]. In these experiments, the recombination occurred on a time scale comparable to the electron thermalization time so the shape of the initial electron energy distribution is important. It is therefore desirable to examine not only the plasma heating effects in Li but to further explore the effects the non-Maxwellian distribution has on three-body recombination.

To do this it is necessary to calculate the rate for an arbitrary energy distribution. Using the principle of detailed balance and the usual Lotz formula for the electron collisional ionization cross section for a bound electron in a state with ionization potential, I_p [20], it can be shown that the three-body recombination rate for an arbitrary electron energy distribution $f(E)$ is [21]

$$W_{\rm rec}(f) = n_i n_e^2 \frac{h^3}{8\pi m_e^2} g \frac{a_i q_i}{I_p} \int_{I_p}^{\infty} \frac{\ln(E/I_p)}{E-I_p} \times \left[\int_0^{E-I_p} \frac{f(E_2) f(E-E_2-I_p)}{E_2^{1/2}(E-E_2-I_p)^{1/2}} dE_2 \right] dE, \quad (5)$$

where a_i is the constant given for the ionization cross section in Ref. [20], n_i, is the ion density, n_e is the electron density, g is the degeneracy of the state into which the recombination event occurs, and q_i is the number of electrons in the ion's outer shell. For a Maxwellian distribution, given by $f_{\rm Max}(E) = 2\pi^{-1/2} n_e (kT_e)^{-3/2} E^{1/2} \exp[-E/kT_e]$, Eq. (5) can be evaluated analytically. The result is the well known formula for the three-body recombination,

$$W_{\rm rec}^{\rm (Max)}(kT_e) = n_i n_e^2 \frac{h^3}{2\pi^2 m_e^2} g \frac{a_i q_i}{I_p} \frac{1}{(kT_e)^2} \times e^{I_p/kT_e} \mathcal{E}_1(I_p/kT_e). \quad (6)$$

Here $\mathcal{E}_1(x)$ is the standard exponential integral function.

To gain insight into the effects of the calculated energy distributions on recombination it is informative to introduce the concept of an effective recombination temperature for an electron energy distribution $f(E)$. This effective temperature is defined as that temperature at which the recombination rate of a Maxwellian distribution with that temperature equals the rate of the non-Maxwellian distribution in question. Thus the effective temperature $kT_e^{\rm (eff)}$ is defined from Eqs. (5) and (6) as

$$W_{\rm rec}^{\rm (Max)}(kT_e^{\rm (eff)}) = W_{\rm rec}(f). \quad (7)$$

To utilize Eq. (5) with the energy distributions calculated in this work, one has to account for the fact that, due to the quantum nature of field ionization, no electrons are actually born with zero energy. Electrons are born with an energy of at least $q\hbar\omega - I_p$ where q is the minimum number of laser photons of energy $\hbar\omega$ required to ionize the ion. The quasiclassical model of the ATI used in the model does not account for this [3]. Therefore the lower limit of integration in Eq. (5) for the calculations presented below is set to $q\hbar\omega - I_p$ instead of 0 to account for this offset.

The calculated temperature as a function of density in Li is shown in Fig. 3(a) for both 400 and 800 nm pulses. The trend is similar to that of He with collisional heating important above 10^{19} cm^{-3}. The dramatic effect that collisions have on the electron distribution is illustrated in Fig. 3(b) where the calculated distributions produced from the ionization of Li by a 400 nm pulse with a peak intensity of 10^{17} W/cm^2 are plotted for an ion density of 10^{17} and 10^{19} cm^{-3}. The Li distribution is quite strongly peaked at $E=0$ for the low density distribution due to the low intensity required to ionize the first electron ($I_p = 5.4$ eV). Using the definition of

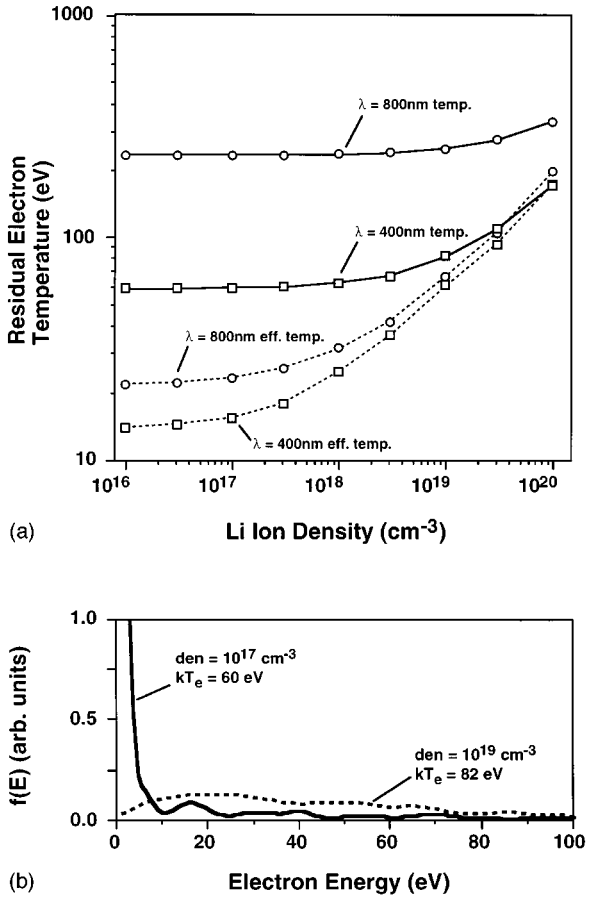

FIG. 3. (a) Calculated actual and effective recombination temperature as a function of density in Li for 400 and 800 nm pulses with peak intensity of 10^{17} W/cm^2. (b) Calculated distributions produced from the ionization of Li by a 400 nm pulse.

Eq. (7), the effective recombination temperature for the calculated energy distributions in Li for 400 and 800 nm light are plotted in Fig. 3(a) as well. Here, the ionization potential of the Li^{2+} ground state (122 eV) is used in Eq. (5) to facilitate the derivation of numerical results, though actual recombination will occur into a range of energy levels with binding energy ranging from 0 to the ground state energy. At low density the effective recombination temperature is much lower than the ''actual'' temperature. While the actual temperature of the Li plasma produced by 400 nm light is roughly 60 eV at a density below 1×10^{19} cm^{-3}, the recombination temperature is much lower; $\sim$15 eV at a density $<1\times10^{18}$ cm^{-3}. The plasma produced with 800 nm pulses exhibits a similar behavior. This result seems to be in line with the observations of Donnelly and co-workers that the recombination in Li ionized by 400 nm light was consistent with an electron temperature of <10 eV [2,12].

The effective temperature, like the actual temperature, is set by the shape of the energy distribution at low density by the ATI distribution. However, the effective temperature begins to rise due to inverse bremsstrahlung at a lower density than does the actual temperature. At a density of between 10^{17} and 10^{19} cm^{-3} the high collisionality of the cold electrons in the strong peak at $E=0$ that results from ATI undergoes more heating than the majority of the electron distribution. Thus the effective recombination temperature begins to

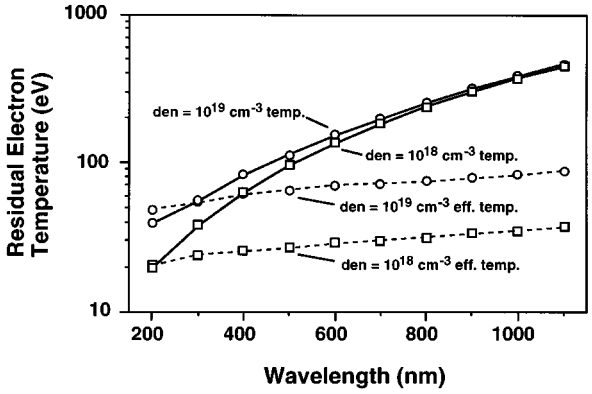

FIG. 4. Calculated actual and effective recombination temperature as a function of laser pulse wavelength in Li at a peak intensity of 10^{17} W/cm^2.

rise, even at a density where the average electron energy is not dramatically changed. This calculation indicates that though it is possible to increase the density of the media from 10^{17} to 10^{19} cm^{-3} without significantly increasing the actual temperature of the plasma, doing this may have a dramatic effect on the recombination rate through collisional heating's redistribution of the electron energy distribution.

The actual temperature of the Li plasma is much higher for 800 nm light than for 400 nm light. This is merely due to the $I\lambda^2$ scaling of the ATI heating exhibited in Eq. (2). This large difference in actual temperature, however, is not reflected in the effective recombination temperature of the plasmas produced by the two wavelengths. The effective temperature at 10^{17} cm^{-3} for 400 nm light is only 15 eV while that of the 800 nm pulse is nearly the same, 20 eV. This is due to the fact that it is the cold electrons near $E=0$ that contribute most strongly to the recombination rate in Eq. (5). The electron energy distributions produced by 400 and 800 nm light both have a strong peak at $E=0$ in a low density plasma, and both therefore have a low effective temperature.

The effect that the wavelength has on the actual and the effective recombination temperature is shown in Fig. 4 for a density of 10^{18} cm^{-3}. The actual temperature rises with increasing wavelength as roughly λ^2. This is due to the scaling of the ATI heating with wavelength as discussed above. The effective temperature (also plotted in Fig. 4), on the other hand, does not show the fast rise with increasing wavelength that the actual temperature exhibits. This is due to the fact that, though the residual temperature of the short wavelength pulses is lower, the collisional heating of the coldest electrons near $E=0$ has been more severe in the distribution produced in the short wavelength pulse than in the long wavelength pulses. The cause of this effect can be seen by considering Eq. (4). Due to the λ^2 scaling of U_p the collision frequency is higher in laser fields of shorter wavelength. Thus collisional heating of the cold electrons is more efficient with short wavelength light. This result seems to indicate that the advantage traditionally accorded to short wavelength pulses in creating a cold plasma for fast recombination may not be as great as simple calculations of ATI heating suggest [3]. Note that the effective recombination temperature of light near 200 nm is roughly the same as that at 400 nm, despite the factor of 4 increase in the actual temperature. This may explain why experiments on the recombination gain in Li at 248 and 400 nm exhibit nearly the same gain [1,2]. The calculation for a density of 10^{19} cm^{-3} is also shown in Fig. 4. The actual temperature is comparable to that at 10^{18} cm^{-3} (except for $\lambda<400$ nm), while the effective temperature is somewhat higher over the entire wavelength range because of greater collisional redistribution of the electron energy function.

In conclusion, the temperature of optically ionized plasmas produced by high intensity 100 fs laser pulses has been investigated by Monte Carlo simulation. The magnitude of heating in He and Li plasmas for intensity in the 10^{16}–10^{17} W/cm^2 range due to inverse bremsstrahlung is found to be unimportant for ion densities below 10^{19} cm^{-3}. However, collisions are found to play an important role in determining the shape of the electron energy distribution at density between 10^{16} and 10^{19} cm^{-3}. At low density the distribution is characteristic of an ATI distribution; at high density the distribution evolves toward that of a Maxwellian. The shift seen in the energy distribution has a dramatic effect on the actual recombination rate. These simulations are in good agreement with a number of recent experimental results and shed light on the interplay of optical ionization and recombination in plasmas of interest for recombination x-ray lasers.

I would like to thank R. W. Lee, T. D. Donnelly, T. E. Glover, R. A. Smith, and M. D. Perry for helpful conversations.

[1] Y. Nagata, K. Midorikawa, S. Kubodera, M. Obara, H. Tashiro, and K. Toyoda, Phys. Rev. Lett. **71**, 3774 (1993).
[2] T. D. Donnelly, L. B. DaSilva, R. W. Lee, S. Mrowka, M. Hofer, and R. W. Falcone, J. Opt. Soc. B **13**, 185 (1996).
[3] N. H. Burnett and P. B. Corkum, J. Opt. Soc. Am. B **6**, 1195 (1989).
[4] B. M. Penetrante and J. N. Bardsley, Phys. Rev. A **43**, 3100 (1991).
[5] S. C. Rae and K. Burnett, Phys. Rev. A **46**, 2077 (1992).
[6] K. A. Janulewicz, M. J. Grout, and G. J. Pert, J. Phys. B **29**, 901 (1996).
[7] T. E. Glover, T. D. Donnelly, E. A. Lipman, A. Sullivan, and R. W. Falcone, Phys. Rev. Lett. **73**, 78 (1994).
[8] W. J. Blyth, S. G. Preston, A. A. Offenberger, M. H. Key, J. S. Wark, Z. Najmudin, A. Modena, A. Djaoui, and A. E. Dangor, Phys. Rev. Lett. **74**, 554 (1995).
[9] T. E. Glover, J. K. Crane, M. D. Perry, R. W. Lee, and R. W. Falcone, Phys. Rev. Lett. **75**, 445 (1995).
[10] P. Pulsifer, J. P. Apruzese, J. Davis, and P. Kepple, Phys. Rev. A **49**, 3958 (1994).
[11] T. D. Donnelly, R. W. Lee, and R. W. Falcone, Phys. Rev. A **51**, R2691 (1995).

[12] D. C. Eder, P. Amendt, L. B. DaSilva, R. A. London, B. J. MacGowan, D. L. Mathews, T. D. Donnelly, R. W. Falcone, and G. L. Strobel, Phys. Plasmas **1**, 1744 (1994).
[13] S. C. Wilks, W. L. Kruer, E. A. Williams, P. Amendt, and D. C. Eder, Phys. Plasmas **2**, 274 (1995).
[14] J. K. Crane, H. Nguyen, T. Ditmire, C. Coverdale, T. E. Glover, M. D. Perry, and Y. Zakharenkov, J. Opt. Soc. Am. B **13**, 89 (1996).
[15] M. V. Ammosov, N. B. Delone, and V. P. Krainov, Zh. Eksp. Teor. Fiz. **91**, 2008 (1986) [Sov. Phys. JETP **64**, 1191 (1986)].
[16] G. J. Pert, Phys. Rev. E **51**, 4778 (1995).
[17] L. Spitzer, *Physics of Fully Ionized Gases* (Interscience, New York, 1967).
[18] R. D. Jones and K. Lee, Phys. Fluids **25**, 2307 (1982).
[19] L. Schlessinger and J. Wright, Phys. Rev. A **20**, 1934 (1979).
[20] W. Lotz, Z. Phys. **216**, 241 (1968).
[21] R. W. Lee (private communication).